5

Deep learning applied to follow-up

Endovascular repair is associated with a significant reduction in perioperative mortality and morbidity compared to open surgery [116]. However, Section 5.1 shows that different types of complications at medium and long- term follow-up can be observed after EVAR in cases of lifelong surveillance [117]. CTAs analysis can be particularly useful in assessing the evolution of aortic anatomy during follow-up. Thus, using an automated segmentation method to extract the aortic lumen in postoperative cases is of great interest. For this purpose, the deep learning pipeline described in Section 3.3 have been trained using a bigger dataset including patients with follow-up. The dataset is composed by patients affected by AAA and TAA. The stent graft is extracted from post-operative acquisitions using a standard intensity-based segmentation approach. Finally, a preliminary work on geometric analysis is introduced to assess changes in aortic anatomy during follow-up.

5.1 Postoperative EVAR follow-up

After EVAR stent-graft implantation, several medium and long term complications have been observed in cases of lifelong patients surveillance [117]. Although EVAR presents reduced perioperative mortality compared to traditial OSR, EVAR follow-up is essential to timely manage and treat any complications.

CTA is the gold standard imaging technique used to identify eventual stent-graft failure (such as stenosis, angulation, stent migration, stent fractures) and endoleaks [117]. Endoleaks are characterized by persistent blood flow outside the endoprosthesis but within the aneurysm sac, and they are the main cause for EVAR failure [118]. Endoleaks can also lead to an increase in the aneurysm diameter over time, with subsequent risk of rupture [119]. CTA imaging provides details of both aortic anatomy and stent-graft appearance. During follow-up evaluations, both the aneurysms diameter and stent-graft appearance are assessed. Since aneurysm shrinkage indicates that the endovascular stent is working properly, the aneurysm size is crucial to determine the success of EVAR intervention [2]. In order to monitor the aneurysm sac size, aneurysm diameter measurements are performed on the follow-up CTAs at regular time intervals to evaluate the anuerysm modifications over time. Nevertheless, some studies have shown that diameter measurements are not sensitive in detecting aneurysm modification after EVAR, while aneurysm volume quantification should be preferred for early diagnosis of patients with growing aneurysms [120, 121]. Although aneurysm volume measurement is superior to maximum diameter measurements, aneurysm volume quantification is too time-expensive for clinical practice [2]. On average, the segmentation time needed to segment the aneurysm sac from CTA ranges from 25 to 40 minutes per patient [59].

5.2 Lumen Segmentation

In this section, a deep learning approach is described to localize and segment the aortic lumen from *preoperative* and *postoperative* CTAs of patients affected by TAA and AAA. As described in detail in Section 3.3, the aortic lumen is first localized in CTA scans, then the identified region of interest (ROI) is segmented using three distinct 2D networks working on axial, sagittal, and coronal planes. Finally, the segmentations obtained from the individual 2D views are combined to provide the final segmentation. In case of postoperative CTAs, the proposed method is also able to segment the stent implanted with thoracic endovascular repair (TEVAR).

Given the TAA dataset, that is composed of pre-operative and post-operative CTA scans, it is necessary to understand whether it is better to use two different networks to segment pre- and post-operative data.

Then, since it is well known that the dataset size has a huge impact on deep learning models performance, in this work we combine all the available datasets (TAA and AAA) together. However, the ground truth segmentations of the two datasets do not present the same characteristics: the segmentations in the TAA dataset only include the thoracic tract whereas those in the AAA dataset extend to the iliacs arteries. Therefore, in order to integrate the AAA and TAA datasets, the model trained on AAA preoperative data (Section 3.3) is applied to the TAA dataset to extend the segmentation to the iliac arteries. This step is necessary in order to facilitate the integration of AAA and TAA datasets and also to extract as much information as possible from the TAA scans.
This datasets integration allows to obtain a DL network capable of segmenting the entire aortic anatomy of TAA/AAA patient from pre/postoperative CTA acquisitions.

5.2.1 Available Datasets

For this work, two different datasets composed of CTA scans have been adopted. All the datasets have been provided by the IRCCS of the Policlinico San Martino Hospital in Genoa under patient's approval.

1. **AAA labelled dataset**
   This dataset has been described in Section 3.3.1. It is composed of 80 preoperative scans of patients affected by AAA. The ground truth segmentations include thoracic, abdominal, and iliac aortic tracts.

2. **TAA labelled dataset**
   The dataset is composed of 84 preoperative and postoperative CTA scans of patients affected by TAA. The ground truth segmentations include the thoraci segment, but they do not include abdominal tract and the iliac arteries. One to four CTA scans are available for each patient.

5.2.2 TAA Lumen Segmentation

As a first step, the TAA labelled dataset is used to train the segmentation model described in Section 3.3. The dataset is composed of 84 CTAs divided into training ($n = 69$), validation ($n = 6$), and test set ($n = 9$). As already mentioned in the previous Section, the TAA dataset may include

Preoperative	DSC	Mean surface distance [mm]
Patient 1	0.958	0.667
Patient 2	0.943	0.638
Patient 3	0.938	0.921
Average	0.946 ± 0.010	0.74 ± 0.15

Table 5.1: Performance of the TAA model on the preoperative test set acquisitions.

Postoperative	DSC	Mean surface distance [mm]
Patient 1	0.944	0,660
Patient 2	0.916	1.140
Patient 3	0.950	0.670
Average	0.937 ± 0.017	0.82 ± 0.27

Table 5.2: Performance of the TAA model on the postoperative test set acquisitions.

multiple CTA scans for each patient. The train-validation-test splitting is implemented in a way that the scans of the same patient are all included into the same set.
Since the dataset is composed of pre-operative and post-operative CTAs, the objective of this preliminary analysis is to understand if it is necessary to develop two separate models depending on whether the scan is pre- or post-operative. Therefore, the TAA dataset of both pre and post-operative CTAs is used to train a deep learning model and the model performance is analyzed to verify if the segmentation performance is different depending on the type of scan.
As it can be noticed from Tables 5.1 and 5.2, the model trained on TAA dataset do not highlight substantial performance differences between pre- and post-operative scans. Thus, a single model can be used to segment pre- and post-operative CTA scans.

5.2.3 TAA and AAA Lumen Segmentation

The dataset size is a key aspect in determining the performance of a deep learning model. Typically, large datasets enable better model performances and reduce data overfitting. Using as much data as possible is crucial to have a final model that performs well on both the training set and unseen data. Since we have collected two different labelled datasets containing CTAs of patients affected by aortic aneurysm (Section 5.2.1), the idea is to merge them to obtain a global larger dataset and to train again the segmentation pipeline described in Section 3.3.

As already explained in Section 5.2.1, the two datasets have been segmented in different way. The AAA dataset has been annotated to train the segmentation network, whereas the TAA dataset has been manually segmented to perform geometric analysis on the thoracic tract. Thus, the TAA segmentations only include the thoracic area of interest.
To create a global model, the two datasets need to be integrated: the idea is to complete the manual segmentations of the TAA dataset by adding the segment of aortic morphology not labeled in the ground truth. Hence, the model trained on the AAA dataset (Section 3.3) is used to make predictions on the TAA scans and to integrate the abdominal tract and the iliac arteries to the ground truth segmentations.
However, since the TAA dataset presents only the thoracic lumen segmentation, the predicted segmentations cannot be evaluated quantitatively in the abdominal and iliac tract. Then, to estimate the goodness of the predicted segmentation and decide whether to integrate the missing parts estimated by the network, the DSC is evaluated in the last tract of thoracic segmentation: if the DSC is considered good with respect to an arbitrary threshold ($DSC > 0.895$), the prediction of the AAA model is added to the original ground truth (Figure 5.1). The AAA dataset and the TAA scans that meet the DSC requirement are merged and used to train a new global model. The adopted approach follows this scheme:

1. Train the model on the actual dataset

2. Use the trained model to make predictions on the TAA scans excluded from the actual dataset ($DSC < 0.895$)

3. Add the TAA scans with $DSC > 0.895$ to the actual dataset, if any

(**a**) (**b**)

Figure 5.1: Prediction of the AAA model on the TAA dataset. In green, the manual segmentation of the thoracic aorta. In red, the segmentation predicted by the AAA model including the abdominal area and the iliac arteries. Two different examples are shown in figure a) and b).

4. If TAA scans have been added to the dataset, go to step 1) and repeat the other steps, otherwise stop the training process.

Table 5.3 shows that this process has been repeated 4 times. After *Iteration 3*, none of the CTAs excluded from the dataset presents a DSC greater than 0.895, so the data inclusion process is terminated.
The global dataset is composed of 80 AAA scans and 40 TAA scans (Table 5.5). More in detail, the AAA dataset includes only pre-operative CTA scans, while the TAA dataset is composed of 10 pre-operative and 30 post-operative CTAs. After the iterative data addition process, the TAA scans in the global dataset extends to the iliac arteries (Figure 5.1). The dataset division into training, validation and test set is shown in Table 5.4. The performances of the trained model are summaryzed in Table 5.6, where the metrics are calculated separately for the pre- and post-operative patients belonging to the test set. As already noticed in the experiment performed on the TAA dataset (Section 5.2.2), the segmentation results obtained for the preoperative and postoperative scans do not show substantial difference.

	Preoperative TAA scans	Postoperative TAA scans	Total scans
Iteration 0	8	16	24
Iteration 1	9	25	34
Iteration 2	10	28	38
Iteration 3	10	30	40

Table 5.3: Evolution of TAA dataset over the iterations.

Dataset	Train	Validation	Test	Total
Iteration 0	84	9	11	104
Iteration 1	93	10	11	114
Iteration 2	95	11	12	118
Iteration 3	97	11	12	120

Table 5.4: Dataset division into train, validation, and test set over the iterations.

Dataset	Preoperative	Postoperative	Total
AAA	80	0	80
TAA	10	30	40
Total	90	30	120

Table 5.5: Final dataset obtained merging AAA dataset and part of the TAA labelled dataset.

Test set	Average DSC	Average Surface Distance [mm]
Preoperative (8 CTAs)	0.929 ± 0.018	0.766 ± 0.162
Postoperative (4 CTAs)	0.930 ± 0.016	0.914 ± 0.262

Table 5.6: Average results obtained on the test set. The scores have been computed separately for pre-operative and post-operative scans.

5.3 Stent Graft Segmentation

During EVAR and TEVAR procedures, one or more endoprosthesis are delivered and positioned in the damaged areas of the aortic lumen. The stent graft is a device that excludes the diseased portion of the aorta from the blood flow, thus reducing the aneurysm sac pressurization. Stent-grafts are composed of a metallic frame covered by synthetic materials.

Since the stent graft is not segmented in the datasets, standard intensity-based approaches are adopted to extract it from the post-operative TAA CTAs. The method is composed of several steps:

1. Given that the stent-graft is surrounded by the diseased aorta, the aortic lumen segmentation predicted the DL-pipeline is dilated with $n = 2$ iterations to get the region of interest for stent-graft segmentation.

2. The dilated lumen segmentation is used to mask the CTA and consider only the areas of interest. Since the endoprosthesis metallic frame can be visualized in the CTA as a bright structure, a simple thresholding algorithm is adopted to extract a preliminary segmentation of the stent. Pixels with Hounsfield Unit (HU) > 800 are labelled as stent-graft, while the others as background. However, calcifications present high intensity values (around 1000 HU) as well; if present, they may be classified as stent-graft.

3. Since calcifications may appear as small disconnected group of pixels in the obtained segmentation, a strategy based on connected components is used to extract only the stent graft from the segmentation. However, if the mesh of the prosthesis is not very thick, the frame components may appear disconnected as well in the preliminary segmentation. To avoid this effect, preliminary segmentation is first dilated with $n = 5$ iterations so that the separated components of the same stent can be connected other and a single connected component can be obtained. Since the stent may present a more or less dense structure, a different number of dilation iterations n may be used. Stents with loose mesh may need a higher dilation parameter, while those with dense mesh may need fewer iterations. In the latter case, using a high dilation parameter could lead to the inclusion of calcifications in the stent segmentation.

4. Only the biggest connected component is kept in the stent-graft dilated

segmentation. Finally, this segmentation is used as a mask on the initial segmentation obtained at step 1). In this way, the size of the stent is not altered by the dilatation process.

5.4 TAA Follow-up Evaluations

Aortic disease represents the 12^{th} leading global cause of death. Descending thoracic aortic aneurysms are a small but significant portion of this pathology. Currently, most TAAs are now repaired by endovascular approach. Short and mid-term data regarding patients undergoing endovascular repair indicate acceptable morbidity and mortality compared with open TAA repair, but long-term follow-up data are still limited [122].
The main disadvantage of TEVAR is the possible occurrence of post-operative procedure-related complications. Most common complications include endoleak formation, migration, and stent graft collapse, which jeopardize the success of the treatment and may result in further intervention [123].
One of the problems related to TEVAR procedure is the possible evolution of landing zones, which are healthy areas of the treated aorta that can become diseased after intervention. While several studies have been conducted on neck diameter evolution for EVAR, studies regarding the effects of the TEVAR intervention are still limited. In addition, other problems may arise due to the tendency of the prosthesis to straighten.
In their study, Yau et. all [124] showed that aortic neck dilatation is quite common after TEVAR, and that the diameter modifications can occur in the proximal landing zone. These findings highlight the importance of close follow-up in TEVAR patients. However, the variability of aortic diameter measurements is widely described in the literature: comparison of follow-up examinations requires measurements at the same locations, and diameter measurements usually depend on the multiplanar reconstruction orthogonal to the aortic centerline [125].
Thus, the definition of an automated pipeline to measure aortic diameters in the areas of interest would reduce the issues related to measurement variability and would speed up comparative analyses between follow-up acquisitions.

The aim of this *preliminary* work is to develop a method to analyze the geometry of the aortic anatomy in order to study its possible modification during follow-up acquisitions. More in detail, the lumen diameters are mea-

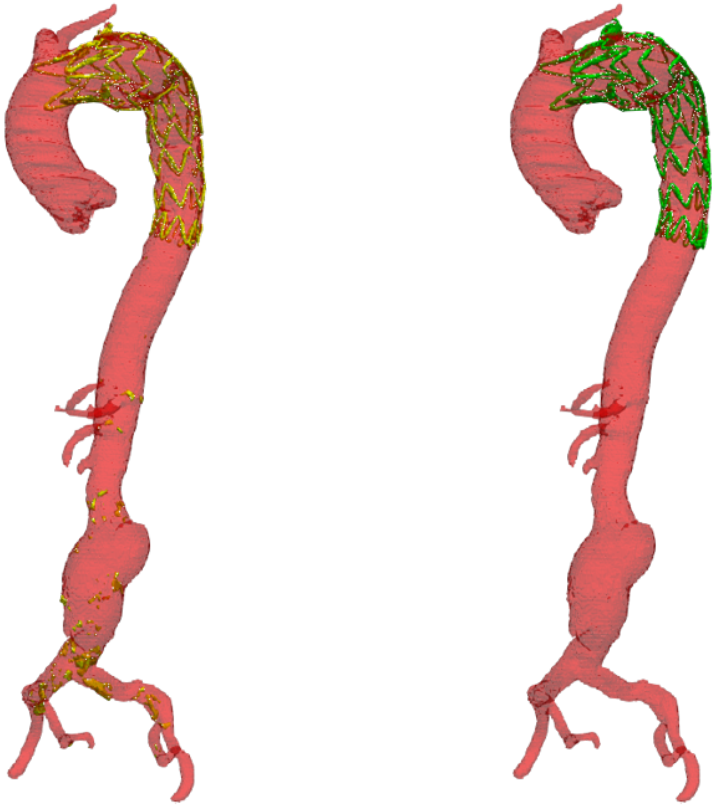

(**a**) (**b**)

Figure 5.2: Stent post-processing. The stent segmentation obtained with binary thresholding is represented in a). The stent segmentation is displayed in yellow, the aorta in red. The initial segmentation also includes some calcifications that are located in the abdominal and iliac areas. In Figure b), the initial segmentation is processed considering connected components, and the result is displayed in green.

sured in the first 2 cm and last 2 cm of stent graft (the landing zones). In addition, the average curvature at the landing zone and the overall tortuosity of the aorta within the stent graft are also calculated. These measurements are repeated at the various time-points of follow-up, with the goal of assessing whether the aortic diameters in the landing zones evolve over time.

5.4.1 Dataset

This study is performed using a database of 15 patients who underwent TEVAR treatment at IRCCS Ospedale Policlinico San Martin (Genoa, Italy). Regarding pathology, only patients with thoracic aneurysm are included in the study, while patients with aortic dissections are excluded. Since the goal of this work is to analyze the evolution of lumen diameters at various follow-up, only patients who have two or more postoperative CT scans are included in the study. These patients are part of the dataset of TAA scans described in Section 5.2.1 (*i.e.*, dataset number 2). In the analyzed dataset, 69% of patients were male, 31% were female. The mean age is 74 ± 4 years. The dataset includes a total of 42 scans: 10 scans are acquired 1 month after surgery, 13 scans are acquired at 1 year after surgery, 11 scans are acquired at 2 years, and 8 scans are acquired at 3 years.
Each CT scan is provided with the corresponding lumen segmentation. The segmentation is obtained using the implemented segmentation pipeline and is manually modified by the expert when necessary. Stent segmentation is automatically performed using the procedure described in Section 5.3. Because most geometric analysis is performed in the first and last 2 cm of the stent (i.e., the *landing zones*), the identification of the stent graft in the CT scan is a critical step. Therefore, the segmentations provided by the automated method are visually checked by an expert and modified where necessary.

The study was approved by the Liguria Regional Ethics Committee (Comitato Etico Regionale Liguria) on October 20^{th}, 2021 (Ref. internal No: 451/2021).

5.4.2 Methods

Geometric analysis is entirely performed using the VMTK library [81]. The next sections will briefly present the steps used to analyze the single postop-

erative CTA acquisition. Then, for patients with multiple follow-up acquisitions, the measurements obtained at various time-points are compared to identify any aortic issue.

Centerline Computation

The first key step in the developed pipeline involves the extraction of the lumen centerline. The lumen segmentation is first pre-processed by keeping only the largest connected component and removing the disconnected components. The polygonal model of the lumen is created using Marching Cubes algorithm from the lumen segmentation. A polygonal model is obtained from the stent-graft segmentation as well. Then, the anatomical landmarks that were manually identified by the experts and used to train the network described in Section X are used as seed points to extract the centerline from the full 3D model of the lumen. Since we are interested in analyzing the thoracic tract, we consider as source seed the landmark located in the aortic bulb, and the landmark located in the renal bifurcation as the target seed (Figure 5.3). Since the geometric analysis must be limited to the stent graft area, a convex hull is built from the stent polygon and used to isolate the portion of the centerline of our interest Figure 5.4. In order to focus on the damaged area within the stent graft, only the aortic sections that are contained in the convex hull are maintained for the analysis. Then, a smaller centerline is computed within the area of interest (Figure 5.5).

Tortuosity and Length Computation

Some of the key aspects used to assess aortic changes during follow-up are aortic length within the stent-graft and tortuosity. An increase of centerline length over time, given two or more stents implanted, means a mutual migration of the stents over each other and thus a decrease in the overlap zone. In addition, tortuosity has been identified as a risk factor for type 1b endoleak [126], so monitoring tortuosity over follow-up acquisitions is critical. Moreover, centerline tortuosity represent an important factor for different cardiovascular diseases [127]. Given the centerline length L and the shortest distance between the two centerline endpoints ED, the centerline tortuosity T is defined as follows:

$$T = \frac{L}{ED} - 1 \tag{5.1}$$

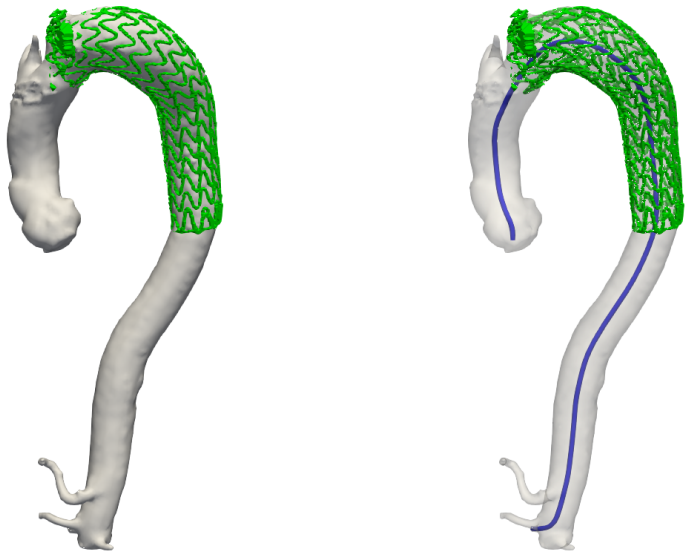

(**a**) (**b**)

Figure 5.3: 3D model of postoperative lumen and stent. In a), the thoracic lumen and the stent graft are represented in white and green respectively. In figure b), the computed aortic centerline is represented in blue.

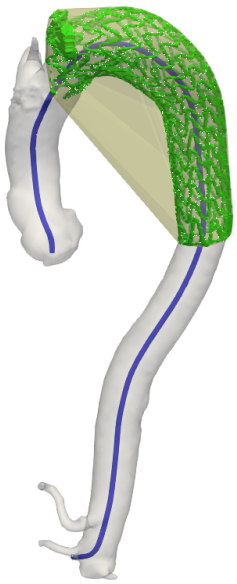

Figure 5.4: Convex hull created from the stent-graft segmentation. The convex hull is represented in yellow, while the stent-graft and the aortic centerline are represented in green and white respectively.

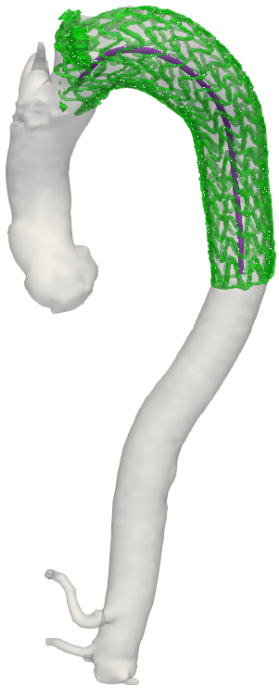

Figure 5.5: Geometrical analysis in the damaged aortic area. Given the convex hull represented in Figure 5.4, only the centerline contained in the hull is maintained for the analysis (in purple).

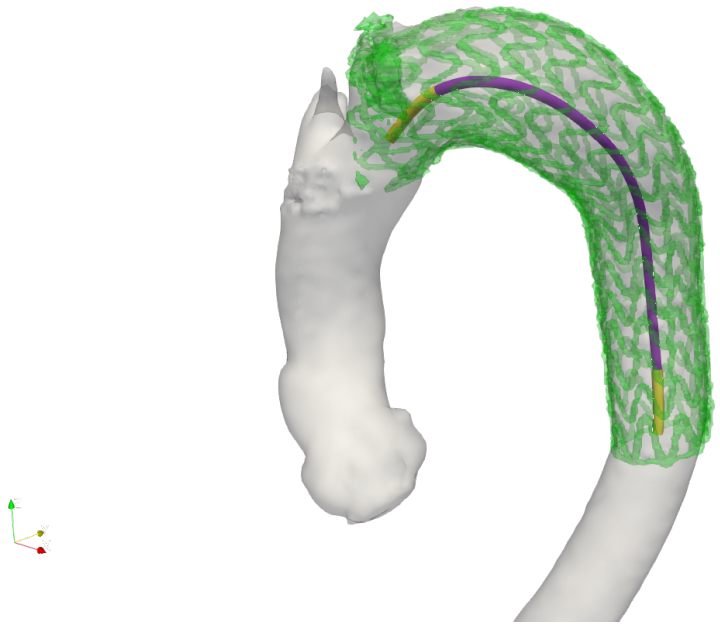

Figure 5.6: Geometrical analysis in the landing zones. Two centerlines are considered (yellow): one includes the first 2 cm and the other the last 2 cm of the centerline within the stent-graft. The average curvature and diameters are evaluated in both segments.

Landing Zones Analysis

Since the main purpose of the work is to evaluate geometric changes in the landing zones, parameters such as mean diameter and curvature in the first and last 2 cm of the stents are calculated. To obtain these indices, two small centerlines are extracted from the centerline of the lumen within the stent: the first describes the proximal landing zone, the second the distal landing zone (Figure 5.6). The values of curvature and diameters are obtained using VMTK library and averaged.

5.4.3 Results

The geometric analysis was applied to a dataset of 15 patients with postoperative CTA acquisitions. Table 5.7 shows the result obtained on a single patient. For this patient, the measured data show that over time the proximal and distal landing zones evolve: the diameters increase and in the future

	1 Month Acquisition	1 Year Acquisition	2 Year Acquisition
Stent lenght [mm]	166.6	168.8	172.8
Aortic tortuosity	0.39	0.36	0.34
Max diameter first 2 cm [mm]	40.0	43.6	45.4
Min diameter first 2 cm [mm]	37.3	40.6	41.64
Max diameter last 2 cm [mm]	27.8	31.8	34.6
Min diameter last 2 cm [mm]	24.5	28.0	31.7
Curvature first 2 cm	0.012	0.008	0.008
Curvature last 2 cm	0.015	0.012	0.017

Table 5.7: Post-operative analysis of a patient with follow-up at one month, one year, and two years after surgery.

an endoleak could develop with need for retreatment. Also, as expected, stent length increases while aortic tortuosity decreases.

Figure 5.7 presents the maximum diameter measurements in the landing zones during the various follow-up. The data shows that in a selected population of aneurysmal patients undergoing TEVAR, the proximal and distal neck tends to evolve during follow-up. The mean landing zone diameters computed at 1 month, 1 year, 2 years and 3 years follow-up are summarised in Table 5.8. The mean diameter increases across follow-up acquisitions.

5.4.4 Conclusions

The results obtained on the geometrical analysis only have a preliminary nature, because the analyzed dataset is small and the number of acquisitions per patient is different. Nevertheless, these preliminary results specifically allowed to observe the expected trend, despite the small dataset. In addi-

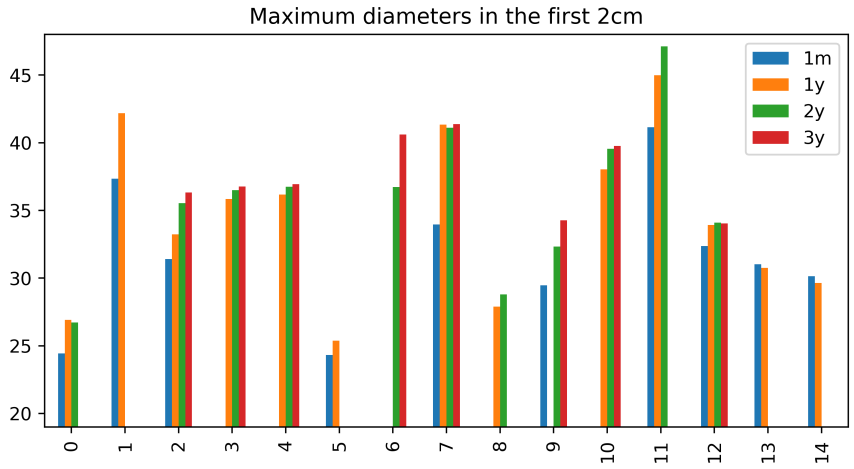

(**a**)

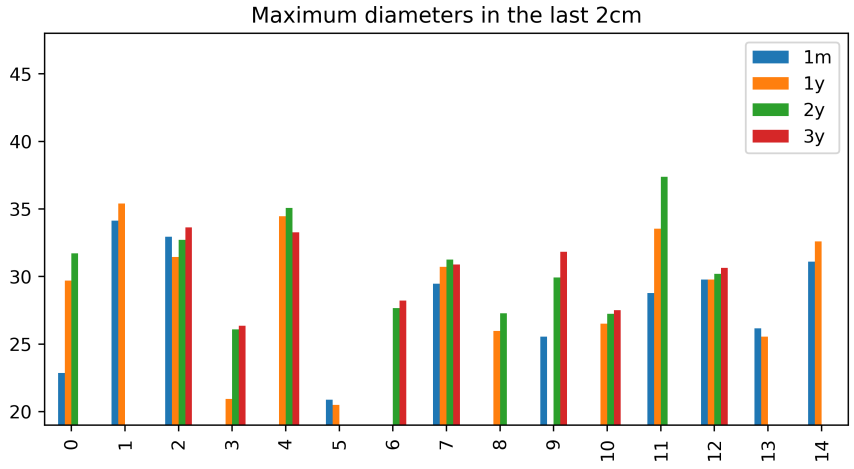

(**b**)

Figure 5.7: Maximum diameters analysis. (a) Maximum diameters in the first 2cm of the stented aorta . (b) Maximum diameters in the last 2cm of the stented aorta. The diameters are reported on the y axis and measured in mm, while patients IDs are reported on the x axis.

	Max diameter first 2 cm [mm]	Min diameter first 2 cm [mm]	Max diameter last 2 cm [mm]	Min diameter last 2 cm [mm]
1 Month Acquisition	31.56 ± 4.91	29.42 ± 4.53	28.16 ± 4.04	25.74 ± 4.02
1 Year Acquisition	34.33 ± 5.92	31.01 ± 5.38	29.00 ± 4.63	26.72 4.12
2 Year Acquisition	35.92 ± 5.38	32.42 ± 4.98	30.59 ± 3.35	27.59 ± 3.20
3 Year Acquisition	37.51 ± 2.60	33.23 ± 2.61	30.29 ± 2.51	27.83 ± 1.83

Table 5.8: Mean landing zones diameters at different follow-up.

tion, this study highlighted the possibility to compare aortic diameters at different levels to provide information about possible aneurysmal dilatation in the distal and proximal zones.
In future developments it will be necessary to increase the dataset and use a statistical test (*t-test*) to verify that the diameter in the landing zones actually increases during the follow-up. The same approach will be used to analyze how the other geometric parameters (length, tortuosity, etc.) vary over time. In addition, the segmentation network described in Section 3.4.3 will be trained to extract the thrombus from postoperative CTA scans. In this way, it will be possible to compute the volumme variation of the aneurysm sac during follow-up acquisitions thus assessing the efficacy of the EVAR/TEVAR treatment.

6

Conclusions

In recent years, new artificial intelligence technologies have been designed, developed and deployed in the medical and clinical domains. With the increasing amount of available medical data, there is a strong need for automated methods that can process information automatically, supporting clinicians. The goal of this thesis has been to propose and validate deep learning methodologies designed to support the various phases of endovascular treatment. Thus, the methodologies proposed in this thesis are aimed at solving specific image processing problems related to the endovascular domain.

In the context of *pre-operative* applications, a novel pipeline has been proposed to allow a fully automated identification and segmentation of the aortic lumen and intraluminal thrombus from CTA scans. Given the automatic segmentations, geometric evaluations of the diameters are performed to evaluate and monitor the preoperative morphology.
This work has allowed for faster segmentation and automation of the aortic diameter measurement procedure, which is subject to intra- and inter-operator variability. Future developments would need to have a larger database based on multi-hospital collaboration to make the developed models more robust. In addition, the developed segmentation method could be put into a multi-user accessible platform to make it accessible from different users. In the context *intra-operative* endovascular applications, we have focused on the aortic deformations caused by tools-tissue interactions. A deep learning model has been trained as a surrogate of finite element analysis to enable faster predictions of the intra-operative aortic deformations induced by

stiff tools insertion. This proof-of-concept work showed promising results, demonstrating the feasibility of using deep learning as a FEA surrogate and overcoming the FEA limits in terms of computational time. In future developments, a bigger dataset will be used to train the model and the DL predictions will be compared to the intraoperative aortic deformations observed in fluoroscopy images.

Finally, the last part of this work deals with *post-operative* endovascular applications. In this context, a DL model is trained to perform lumen segmentation from both preoperative and postoperative CTA scans. In addition, automatic geometric analysis of follow-up TAA scans is performed to verify whether and how the aortic anatomy changes in the landing zones during post-TEVAR follow-up acquisitions. This work speeds up the geometric analysis of aortic anatomy and makes measurements completely operator-independent, facilitating the comparison of these measurements during follow-ups. In future work, as for the *pre-operative* applications, it will be necessary to use larger and possibly multi-center datasets to perform model training and geometric analysis. In addition, it will be useful to include automatic thrombus segmentation from postoperative images as well, so that we can assess how the volume of the aneurysmal sac evolves during follow-ups.

The thesis was conducted in a multidisciplinary setting, integrating the medical and research side with the industry side as well. The methodologies developed in this thesis will be further expanded to be integrated into a support tool for clinical practice in the vascular field. Applying these DL-based methodologies will allow to automate the diagnostic-therapeutic process. Since aortic diseases have serious consequences in terms of mortality and complications, we expect that such clinical tool will have a strong impact on the quality of life of patients. Thus, the proposed work leaves the door open for future developments related to current and future challenges in the endovascular field.

Ringraziamenti

Vorrei dedicare questo piccolo spazio alle persone che mi hanno accompagnato in questo percorso. Non sono brava con queste cose, ma farò del mio meglio.

Innanzitutto vorrei ringraziare Giovanni Spinella, Michele Conti, Curzio Basso e Mario Esposito, che mi hanno guidato e supportato durante questo percorso insegnandomi davvero tantissimo. Sono stati per me un esempio da seguire e un punto di riferimento importante.

Un grazie speciale anche a tutti i colleghi, e soprattutto amici, del gruppo di Camelot, con cui è stato un piacere collaborare durante il periodo di dottorato. Ringrazio in particolare Danilo, per le risate e per il supporto continuo anche nei periodi più complicati.

Un ringraziamento particolare va alle mie tesiste, Elena e Francesca, con cui è stato veramente un piacere collaborare e il cui contributo è stato fondamentale per lo sviluppo di questa tesi.

Ringrazio i miei amici, per esserci sempre stati. Ringrazio le mia famiglia, per il supporto e l'amore smisurato: poter condividere con voi questo traguardo è il premio più grande.

Per ultimo (ma ovviamente non per importanza) un grazie gigantesco a David, per essere la mia roccia e il mio punto fermo sia nei momenti belli che nei momenti difficili. Mille parole non basterebbero per dire quanto sono grata di averti nella mia vita.

Alice

7

List of Publications

International Journals

- Fantazzini, Alice, et al. "3D automatic segmentation of aortic computed tomography angiography combining multi-view 2D convolutional neural networks." Cardiovascular engineering and technology 11.5 (2020): 576-586.
- Brutti, Francesca, Fantazzini, Alice, et al. "Deep Learning to Automatically Segment and Analyze Abdominal Aortic Aneurysm from Computed Tomography Angiography." Cardiovascular Engineering and Technology (2022): 1-13.

Conferences

- Fantazzini, Alice, et al. "Deep learning to estimate the arterial straightening induced by stiff guidewires during EVAR." Abstract accepted at ESBiomech Conference 2021
- Fantazzini, Alice, et al. "Deep learning to support endovascular surgical procedures." Abstract accepted at Italian Chapter of the European Society of Biomechanics X Meeting 2021.

Bibliography

[1] Emile Saliba, Ying Sia, Annie Dore, and Ismael El Hamamsy, "The ascending aortic aneurysm: When to intervene?," *IJC Heart & Vasculature*, vol. 6, pp. 91–100, 2015.

[2] Zhong-Hua Sun, "Abdominal aortic aneurysm: Treatment options, image visualizations and follow-up procedures," *Journal of geriatric cardiology: JGC*, vol. 9, no. 1, pp. 49, 2012.

[3] Maya J Salameh, James H Black III, and Elizabeth V Ratchford, "Thoracic aortic aneurysm," *Vascular Medicine*, vol. 23, no. 6, pp. 573–578, 2018.

[4] Wikipedia, "Thoracic aortic aneurysm," https://en.wikipedia.org/wiki/Thoracic_aortic_aneurysm.

[5] Health University of Utah, "Thoracic aortic aneurysm (taa)," https://healthcare.utah.edu/cardiovascular/programs/aortic-disease/thoracic-aortic-aneurysm/.

[6] JC Parodi, JC Palmaz, and HD Barone, "Transfemoral intraluminal graft implantation for abdominal aortic aneurysms," *Annals of vascular surgery*, vol. 5, no. 6, pp. 491–499, 1991.

[7] RM Greenhalgh and EVAR The, "Comparison of endovascular aneurysm repair with open repair in patients with abdominal aortic aneurysm (evar trial 1), 30-day operative mortality results: randomised controlled trial," *The Lancet*, vol. 364, no. 9437, pp. 843–848, 2004.

[8] Sharath Chandra Vikram Paravastu, Rubaraj Jayarajasingam, Rachel Cottam, Simon J Palfreyman, Jonathan A Michaels, and Steven M

Thomas, "Endovascular repair of abdominal aortic aneurysm," *Cochrane Database of Systematic Reviews*, , no. 1, 2014.

[9] David C Brewster, Jack L Cronenwett, John W Hallett Jr, K Wayne Johnston, William C Krupski, and Jon S Matsumura, "Guidelines for the treatment of abdominal aortic aneurysms: report of a subcommittee of the joint council of the american association for vascular surgery and society for vascular surgery," *Journal of vascular surgery*, vol. 37, no. 5, pp. 1106–1117, 2003.

[10] Elliot L Chaikof, Mark F Fillinger, Jon S Matsumura, Robert B Rutherford, Geoffrey H White, Jan D Blankensteijn, Victor M Bernhard, Peter L Harris, K Craig Kent, James May, et al., "Identifying and grading factors that modify the outcome of endovascular aortic aneurysm repair," *Journal of vascular surgery*, vol. 35, no. 5, pp. 1061–1066, 2002.

[11] Sydney Vascular Surgery, "Abdominal aortic aneurysm," https://www.sydneyvascularsurgery.com.au/abdominal-aortic-aneurysm.html.

[12] Dinggang Shen, Guorong Wu, and Heung-Il Suk, "Deep learning in medical image analysis," *Annual review of biomedical engineering*, vol. 19, pp. 221–248, 2017.

[13] Towards Data Science, "A "weird" introduction to deep learning," 2018, https://towardsdatascience.com/a-weird-introduction-to-deep-learning-7828803693b0.

[14] Warren S McCulloch and Walter Pitts, "A logical calculus of the ideas immanent in nervous activity," *The bulletin of mathematical biophysics*, vol. 5, no. 4, pp. 115–133, 1943.

[15] Frank Rosenblatt, *The perceptron, a perceiving and recognizing automaton Project Para*, Cornell Aeronautical Laboratory, 1957.

[16] Marvin Minsky and Seymour Papert, "An introduction to computational geometry," *Cambridge tiass., HIT*, 1969.

[17] Kunihiko Fukushima, "Neocognitron: A hierarchical neural network capable of visual pattern recognition," *Neural networks*, vol. 1, no. 2, pp. 119–130, 1988.

[18] Christopher M Bishop, *Pattern recognition and machine learning*, springer, 2006.

[19] Maryam M Najafabadi, Flavio Villanustre, Taghi M Khoshgoftaar, Naeem Seliya, Randall Wald, and Edin Muharemagic, "Deep learning applications and challenges in big data analytics," *Journal of big data*, vol. 2, no. 1, pp. 1–21, 2015.

[20] Weibo Liu, Zidong Wang, Xiaohui Liu, Nianyin Zeng, Yurong Liu, and Fuad E Alsaadi, "A survey of deep neural network architectures and their applications," *Neurocomputing*, vol. 234, pp. 11–26, 2017.

[21] Yann LeCun, Léon Bottou, Yoshua Bengio, and Patrick Haffner, "Gradient-based learning applied to document recognition," *Proceedings of the IEEE*, vol. 86, no. 11, pp. 2278–2324, 1998.

[22] I. Goodfellow, Y. Bengio, and A. Courville, *Deep learning*, MIT Press, 2016.

[23] Matthew Stewart, "Simple introduction to convolutional neural networks," *Towards Data Science*, vol. 27, 2019.

[24] MathWorks, "Convolutional neural network: 3 things you need to know," https://it.mathworks.com/discovery/convolutional-neural-network-matlab.html.

[25] Olaf Ronneberger, Philipp Fischer, and Thomas Brox, "U-net: Convolutional networks for biomedical image segmentation," in *International Conference on Medical image computing and computer-assisted intervention*. Springer, 2015, pp. 234–241.

[26] S Kevin Zhou, Hayit Greenspan, Christos Davatzikos, James S Duncan, Bram Van Ginneken, Anant Madabhushi, Jerry L Prince, Daniel Rueckert, and Ronald M Summers, "A review of deep learning in medical imaging: Imaging traits, technology trends, case studies with progress highlights, and future promises," *Proceedings of the IEEE*, 2021.

[27] Ravi Aggarwal, Viknesh Sounderajah, Guy Martin, Daniel SW Ting, Alan Karthikesalingam, Dominic King, Hutan Ashrafian, and Ara Darzi, "Diagnostic accuracy of deep learning in medical imaging: a

systematic review and meta-analysis," *NPJ digital medicine*, vol. 4, no. 1, pp. 1–23, 2021.

[28] Berkman Sahiner, Aria Pezeshk, Lubomir M Hadjiiski, Xiaosong Wang, Karen Drukker, Kenny H Cha, Ronald M Summers, and Maryellen L Giger, "Deep learning in medical imaging and radiation therapy," *Medical physics*, vol. 46, no. 1, pp. e1–e36, 2019.

[29] Samir S Yadav and Shivajirao M Jadhav, "Deep convolutional neural network based medical image classification for disease diagnosis," *Journal of Big Data*, vol. 6, no. 1, pp. 1–18, 2019.

[30] Sertan Serte, Ali Serener, and Fadi Al-Turjman, "Deep learning in medical imaging: A brief review," *Transactions on Emerging Telecommunications Technologies*, p. e4080, 2020.

[31] Pranav Rajpurkar, Jeremy Irvin, Kaylie Zhu, Brandon Yang, Hershel Mehta, Tony Duan, Daisy Ding, Aarti Bagul, Curtis Langlotz, Katie Shpanskaya, et al., "Chexnet: Radiologist-level pneumonia detection on chest x-rays with deep learning," *arXiv preprint arXiv:1711.05225*, 2017.

[32] Mohammad Hesam Hesamian, Wenjing Jia, Xiangjian He, and Paul Kennedy, "Deep learning techniques for medical image segmentation: achievements and challenges," *Journal of digital imaging*, vol. 32, no. 4, pp. 582–596, 2019.

[33] Hyunkwang Lee, Fabian M Troschel, Shahein Tajmir, Georg Fuchs, Julia Mario, Florian J Fintelmann, and Synho Do, "Pixel-level deep segmentation: artificial intelligence quantifies muscle on computed tomography for body morphometric analysis," *Journal of digital imaging*, vol. 30, no. 4, pp. 487–498, 2017.

[34] Kenny H Cha, Lubomir Hadjiiski, Ravi K Samala, Heang-Ping Chan, Elaine M Caoili, and Richard H Cohan, "Urinary bladder segmentation in ct urography using deep-learning convolutional neural network and level sets," *Medical physics*, vol. 43, no. 4, pp. 1882–1896, 2016.

[35] Hongyoon Choi and Kyong Hwan Jin, "Fast and robust segmentation of the striatum using deep convolutional neural networks," *Journal of neuroscience methods*, vol. 274, pp. 146–153, 2016.

[36] Mehmet Ufuk Dalmış, Geert Litjens, Katharina Holland, Arnaud Setio, Ritse Mann, Nico Karssemeijer, and Albert Gubern-Mérida, "Using deep learning to segment breast and fibroglandular tissue in mri volumes," *Medical physics*, vol. 44, no. 2, pp. 533–546, 2017.

[37] Tuan Anh Ngo, Zhi Lu, and Gustavo Carneiro, "Combining deep learning and level set for the automated segmentation of the left ventricle of the heart from cardiac cine magnetic resonance," *Medical image analysis*, vol. 35, pp. 159–171, 2017.

[38] Amal Farag, Le Lu, Holger R Roth, Jiamin Liu, Evrim Turkbey, and Ronald M Summers, "A bottom-up approach for pancreas segmentation using cascaded superpixels and (deep) image patch labeling," *IEEE Transactions on Image Processing*, vol. 26, no. 1, pp. 386–399, 2016.

[39] Peijun Hu, Fa Wu, Jialin Peng, Ping Liang, and Dexing Kong, "Automatic 3d liver segmentation based on deep learning and globally optimized surface evolution," *Physics in Medicine & Biology*, vol. 61, no. 24, pp. 8676, 2016.

[40] AC Lobato and P Puech-Leao, "Predictive factors for rupture of thoracoabdominal aortic aneurysm," *Journal of vascular surgery*, vol. 27, no. 3, pp. 446–453, 1998.

[41] Stefano Giardina, Bianca Pane, Giovanni Spinella, Giuseppe Cafueri, Mara Corbo, Pascale Brasseur, Giovanni Orengo, and Domenico Palombo, "An economic evaluation of an abdominal aortic aneurysm screening program in italy," *Journal of vascular surgery*, vol. 54, no. 4, pp. 938–946, 2011.

[42] Rachel Claridge, Sam Arnold, Neil Morrison, and André M van Rij, "Measuring abdominal aortic diameters in routine abdominal computed tomography scans and implications for abdominal aortic aneurysm screening," *Journal of vascular surgery*, vol. 65, no. 6, pp. 1637–1642, 2017.

[43] RAP Scott, KA Vardulaki, NM Walker, NE Day, SW Duffy, and HA Ashton, "The long-term benefits of a single scan for abdominal aortic aneurysm (aaa) at age 65," *European Journal of Vascular and Endovascular Surgery*, vol. 21, no. 6, pp. 535–540, 2001.

[44] HW Kniemeyer, T Kessler, PU Reber, HB Ris, H Hakki, and MK Widmer, "Treatment of ruptured abdominal aortic aneurysm, a permanent challenge or a waste of resources? prediction of outcome using a multi-organ-dysfunction score," *European Journal of Vascular and Endovascular Surgery*, vol. 19, no. 2, pp. 190–196, 2000.

[45] Abeera Abbas, A Smith, M Cecelja, and M Waltham, "Assessment of the accuracy of aortascan for detection of abdominal aortic aneurysm (aaa)," *European Journal of Vascular and Endovascular Surgery*, vol. 43, no. 2, pp. 167–170, 2012.

[46] Mads Liisberg, Axel C Diederichsen, and Jes S Lindholt, "Abdominal ultrasound-scanning versus non-contrast computed tomography as screening method for abdominal aortic aneurysm–a validation study from the randomized dancavas study," *BMC medical imaging*, vol. 17, no. 1, pp. 1–8, 2017.

[47] H Hafez, PS Druce, and HA Ashton, "Abdominal aortic aneurysm development in men following a "normal" aortic ultrasound scan," *European Journal of Vascular and Endovascular Surgery*, vol. 36, no. 5, pp. 553–558, 2008.

[48] Stephanie M Tomee, Niki Lijftogt, Anco Vahl, Jaap F Hamming, and Jan HN Lindeman, "A registry-based rationale for discrete intervention thresholds for open and endovascular elective abdominal aortic aneurysm repair in female patients," *Journal of vascular surgery*, vol. 67, no. 3, pp. 735–739, 2018.

[49] C Mora, C Marcus, C Barbe, F Ecarnot, and A Long, "Measurement of maximum diameter of native abdominal aortic aneurysm by angio-ct: reproducibility is better with the semi-automated method," *European Journal of Vascular and Endovascular Surgery*, vol. 47, no. 2, pp. 139–150, 2014.

[50] N Rudarakanchana, CD Bicknell, NJ Cheshire, N Burfitt, A Chapman, M Hamady, and JT Powell, "Variation in maximum diameter measurements of descending thoracic aortic aneurysms using unformatted planes versus images corrected to aortic centerline," *European journal of vascular and endovascular surgery*, vol. 47, no. 1, pp. 19–26, 2014.

[51] Diehm, Baumgartner, Silvestro, Herrmann, Triller, Schmidli, Dai-Do, and Dinkel, "Automated software supported versus manual aorto-iliac diameter measurements in ct angiography of patients with abdominal aortic aneurysms: assessment of inter-and intraobserver variation," *Vasa*, vol. 34, no. 4, pp. 255–261, 2005.

[52] Claude Kauffmann, An Tang, Alexandre Dugas, Éric Therasse, Vincent Oliva, and Gilles Soulez, "Clinical validation of a software for quantitative follow-up of abdominal aortic aneurysm maximal diameter and growth by ct angiography," *European journal of radiology*, vol. 77, no. 3, pp. 502–508, 2011.

[53] Yolanda Bryce, Philip Rogoff, Donald Romanelli, and Ralph Reichle, "Endovascular repair of abdominal aortic aneurysms: vascular anatomy, device selection, procedure, and procedure-specific complications," *Radiographics*, vol. 35, no. 2, pp. 593–615, 2015.

[54] Nikola Fatic, Pasha Normahani, Dejan Mars, Nigel J Standfield, and Usman Jaffer, "Validation of an assessment tool for pre-operative evar planning," *Perfusion*, vol. 33, no. 2, pp. 123–129, 2018.

[55] Rishi Sethi, Akshyaya Pradhan, J Shiv Kumar, Tejas Patel, Sanjay Shah, and Samir Pancholy, "Good clinical practices in cath lab," .

[56] Andrew England and Richard Mc Williams, "Endovascular aortic aneurysm repair (evar)," *The Ulster medical journal*, vol. 82, no. 1, pp. 3, 2013.

[57] Elliot L Chaikof, Ronald L Dalman, Mark K Eskandari, Benjamin M Jackson, W Anthony Lee, M Ashraf Mansour, Tara M Mastracci, Matthew Mell, M Hassan Murad, Louis L Nguyen, et al., "The society for vascular surgery practice guidelines on the care of patients with an abdominal aortic aneurysm," *Journal of vascular surgery*, vol. 67, no. 1, pp. 2–77, 2018.

[58] RM Romarowski, E Faggiano, M Conti, A Reali, S Morganti, and F Auricchio, "A novel computational framework to predict patient-specific hemodynamics after tevar: integration of structural and fluid-dynamics analysis by image elaboration," *Computers & Fluids*, vol. 179, pp. 806–819, 2019.

[59] Fabien Lareyre, Cédric Adam, Marion Carrier, Carine Dommerc, Claude Mialhe, and Juliette Raffort, "A fully automated pipeline for mining abdominal aortic aneurysm using image segmentation," *Scientific reports*, vol. 9, no. 1, pp. 1–14, 2019.

[60] Måns Larsson, Yuhang Zhang, and Fredrik Kahl, "Deepseg: Abdominal organ segmentation using deep convolutional neural networks," in *Swedish Symposium on Image Analysis*, 2016, vol. 2016.

[61] Karen López-Linares, Nerea Aranjuelo, Luis Kabongo, Gregory Maclair, Nerea Lete, Mario Ceresa, Ainhoa García-Familiar, Iván Macía, and Miguel A González Ballester, "Fully automatic detection and segmentation of abdominal aortic thrombus in post-operative cta images using deep convolutional neural networks," *Medical image analysis*, vol. 46, pp. 202–214, 2018.

[62] Karen López-Linares, Inmaculada García, Ainhoa García-Familiar, Iván Macía, and Miguel A González Ballester, "3d convolutional neural network for abdominal aortic aneurysm segmentation," *arXiv preprint arXiv:1903.00879*, 2019.

[63] Julia MH Noothout, Bob D De Vos, Jelmer M Wolterink, and Ivana Išgum, "Automatic segmentation of thoracic aorta segments in low-dose chest ct," in *Medical Imaging 2018: Image Processing*. International Society for Optics and Photonics, 2018, vol. 10574, p. 105741S.

[64] Saba Mohammadi, Mahdi Mohammadi, Vahab Dehlaghi, and Arash Ahmadi, "Automatic segmentation, detection, and diagnosis of abdominal aortic aneurysm (aaa) using convolutional neural networks and hough circles algorithm," *Cardiovascular engineering and technology*, vol. 10, no. 3, pp. 490–499, 2019.

[65] Long Cao, Ruiqiong Shi, Yangyang Ge, Lei Xing, Panli Zuo, Yan Jia, Jie Liu, Yuan He, Xinhao Wang, Shaoliang Luan, et al., "Fully automatic segmentation of type b aortic dissection from cta images enabled by deep learning," *European journal of radiology*, vol. 121, pp. 108713, 2019.

[66] Paul A Yushkevich, Yang Gao, and Guido Gerig, "Itk-snap: An interactive tool for semi-automatic segmentation of multi-modality biomedical images," in *2016 38th Annual International Conference of the IEEE*

Engineering in Medicine and Biology Society (EMBC). IEEE, 2016, pp. 3342–3345.

[67] Xiangrong Zhou, Takaaki Ito, Ryosuke Takayama, Song Wang, Takeshi Hara, and Hiroshi Fujita, "Three-dimensional ct image segmentation by combining 2d fully convolutional network with 3d majority voting," in *Deep Learning and Data Labeling for Medical Applications*, pp. 111–120. Springer, 2016.

[68] Mark Lyksborg, Oula Puonti, Mikael Agn, and Rasmus Larsen, "An ensemble of 2d convolutional neural networks for tumor segmentation," in *Scandinavian Conference on Image Analysis*. Springer, 2015, pp. 201–211.

[69] Calvin R Maurer, Rensheng Qi, and Vijay Raghavan, "A linear time algorithm for computing exact euclidean distance transforms of binary images in arbitrary dimensions," *IEEE Transactions on Pattern Analysis and Machine Intelligence*, vol. 25, no. 2, pp. 265–270, 2003.

[70] Angelo Monteux, "Metrics for semantic segmentation," https://ilmonteux.github.io/2019/05/10/segmentation-metrics.html.

[71] Shuman Jia, Antoine Despinasse, Zihao Wang, Hervé Delingette, Xavier Pennec, Pierre Jaïs, Hubert Cochet, and Maxime Sermesant, "Automatically segmenting the left atrium from cardiac images using successive 3d u-nets and a contour loss," in *International Workshop on Statistical Atlases and Computational Models of the Heart*. Springer, 2018, pp. 221–229.

[72] Matthew Lai, "Deep learning for medical image segmentation," *arXiv preprint arXiv:1505.02000*, 2015.

[73] Zongqing Ma, Xi Wu, Qi Song, Yong Luo, Yan Wang, and Jiliu Zhou, "Automated nasopharyngeal carcinoma segmentation in magnetic resonance images by combination of convolutional neural networks and graph cut," *Experimental and therapeutic medicine*, vol. 16, no. 3, pp. 2511–2521, 2018.

[74] Abhijit Guha Roy, Sailesh Conjeti, Nassir Navab, Christian Wachinger, Alzheimer's Disease Neuroimaging Initiative, et al., "Quicknat: A fully convolutional network for quick and accurate segmentation of neuroanatomy," *NeuroImage*, vol. 186, pp. 713–727, 2019.

[75] Eamon G Kavanagh, Pierce A Grace, Tim M McGloughlin, Barry J Doyle, et al., "The biaxial mechanical behaviour of abdominal aortic aneurysm intraluminal thrombus: classification of morphology and the determination of layer and region specific properties," *Journal of biomechanics*, vol. 47, no. 6, pp. 1430–1437, 2014.

[76] Josu Maiora, Borja Ayerdi, and Manuel Graña, "Random forest active learning for aaa thrombus segmentation in computed tomography angiography images," *Neurocomputing*, vol. 126, pp. 71–77, 2014.

[77] Ho Aik Hong and UU Sheikh, "Automatic detection, segmentation and classification of abdominal aortic aneurysm using deep learning," in *2016 IEEE 12th International Colloquium on Signal Processing & Its Applications (CSPA)*. IEEE, 2016, pp. 242–246.

[78] Caroline Caradu, Benedetta Spampinato, Ana Maria Vrancianu, Xavier Bérard, and Eric Ducasse, "Fully automatic volume segmentation of infrarenal abdominal aortic aneurysm computed tomography images with deep learning approaches versus physician controlled manual segmentation," *Journal of Vascular Surgery*, vol. 74, no. 1, pp. 246–256, 2021.

[79] K Singh, BK Jacobsen, S Solberg, KH Bønaa, S Kumar, R Bajic, and E Arnesen, "Intra-and interobserver variability in the measurements of abdominal aortic and common iliac artery diameter with computed tomography. the tromsø study," *European journal of vascular and endovascular surgery*, vol. 25, no. 5, pp. 399–407, 2003.

[80] Adrien Kaladji, Antoine Lucas, Gaëlle Kervio, Pascal Haigron, and Alain Cardon, "Sizing for endovascular aneurysm repair: clinical evaluation of a new automated three-dimensional software," *Annals of vascular surgery*, vol. 24, no. 7, pp. 912–920, 2010.

[81] Luca Antiga, Marina Piccinelli, Lorenzo Botti, Bogdan Ene-Iordache, Andrea Remuzzi, and David A Steinman, "An image-based modeling framework for patient-specific computational hemodynamics," *Medical & biological engineering & computing*, vol. 46, no. 11, pp. 1097–1112, 2008.

[82] Ivo Wolf, Marcus Vetter, Ingmar Wegner, Thomas Böttger, Marco Nolden, Max Schöbinger, Mark Hastenteufel, Tobias Kunert, and Hans-

Peter Meinzer, "The medical imaging interaction toolkit," *Medical image analysis*, vol. 9, no. 6, pp. 594–604, 2005.

[83] Will Schroeder, Kenneth M Martin, and William E Lorensen, *The visualization toolkit an object-oriented approach to 3D graphics*, Prentice-Hall, Inc., 1998.

[84] Brian B Avants, Nicholas J Tustison, Michael Stauffer, Gang Song, Baohua Wu, and James C Gee, "The insight toolkit image registration framework," *Frontiers in neuroinformatics*, vol. 8, pp. 44, 2014.

[85] William E Lorensen and Harvey E Cline, "Marching cubes: A high resolution 3d surface construction algorithm," *ACM siggraph computer graphics*, vol. 21, no. 4, pp. 163–169, 1987.

[86] Arash Salarian, "Intraclass correlation coefficient (icc)," *MATLAB Cent File Exch*, 2016.

[87] Julia MH Noothout, Bob D de Vos, Jelmer M Wolterink, Tim Leiner, and Ivana Išgum, "Cnn-based landmark detection in cardiac cta scans," *arXiv preprint arXiv:1804.04963*, 2018.

[88] Zimeng Tan, Yongjie Duan, Ziyi Wu, Jianjiang Feng, and Jie Zhou, "A cascade regression model for anatomical landmark detection," in *International Workshop on Statistical Atlases and Computational Models of the Heart*. Springer, 2019, pp. 43–51.

[89] Kenneth S Zurcher, Sailendra G Naidu, Samuel R Money, William M Stone, Richard J Fowl, Grace Knuttinen, Rahmi Oklu, Lisa A Rotellini Coltvet, Daniel Crawford, Matthew R Buras, et al., "Dose reduction using digital fluoroscopy versus digital subtraction angiography in endovascular aneurysm repair: A prospective randomized trial," *Journal of vascular surgery*, vol. 72, no. 6, pp. 1938–1945, 2020.

[90] T Gregory Walker, Sanjeeva P Kalva, Suvranu Ganguli, Rahmi Öklü, Gloria M Salazar, Arthur C Waltman, and Stephan Wicky, "Image optimization during endovascular aneurysm repair," *American Journal of Roentgenology*, vol. 198, no. 1, pp. 200–206, 2012.

[91] B Maurel, A Hertault, J Sobocinski, M Le Roux, T Martin Gonzalez, R Azzaoui, M Midulla, S Haulon, et al., "Techniques to reduce radia-

tion and contrast volume during evar.," *The Journal of cardiovascular surgery*, vol. 55, no. 2 Suppl 1, pp. 123–131, 2014.

[92] A Hertault, B Maurel, J Sobocinski, T Martin Gonzalez, M Le Roux, R Azzaoui, M Midulla, and S Haulon, "Impact of hybrid rooms with image fusion on radiation exposure during endovascular aortic repair," *European Journal of Vascular and Endovascular Surgery*, vol. 48, no. 4, pp. 382–390, 2014.

[93] Daniel Toth, Marcus Pfister, Andreas Maier, Markus Kowarschik, and Joachim Hornegger, "Adaption of 3d models to 2d x-ray images during endovascular abdominal aneurysm repair," in *International Conference on Medical Image Computing and Computer-Assisted Intervention*. Springer, 2015, pp. 339–346.

[94] Lars Stangenberg, Fahad Shuja, Bart Carelsen, Thijs Elenbaas, Mark C Wyers, and Marc L Schermerhorn, "A novel tool for three-dimensional roadmapping reduces radiation exposure and contrast agent dose in complex endovascular interventions," *Journal of vascular surgery*, vol. 62, no. 2, pp. 448–455, 2015.

[95] Blandine Maurel, Adrien Hertault, Teresa Martin Gonzalez, Jonathan Sobocinski, Marielle Le Roux, Jessica Delaplace, Richard Azzaoui, Marco Midulla, and Stéphan Haulon, "Evaluation of visceral artery displacement by endograft delivery system insertion," *Journal of Endovascular Therapy*, vol. 21, no. 2, pp. 339–347, 2014.

[96] Tom WG Carrell, Bijan Modarai, James RI Brown, and Graeme P Penney, "Feasibility and limitations of an automated 2d-3d rigid image registration system for complex endovascular aortic procedures," *Journal of Endovascular Therapy*, vol. 17, no. 4, pp. 527–533, 2010.

[97] Laura Cercenelli, Barbara Bortolani, Guido Tiberi, Chiara Mascoli, Ivan Corazza, Mauro Gargiulo, and Emanuela Marcelli, "Characterization of vessel deformations during evar: a preliminary retrospective analysis to improve fidelity of endovascular simulators," *Journal of surgical education*, vol. 75, no. 4, pp. 1096–1105, 2018.

[98] Blandine Maurel, Teresa Martin-Gonzalez, Debra Chong, Andrew Irwin, Guillaume Guimbretière, Meryl Davis, and Tara M Mastracci, "A prospective observational trial of fusion imaging in infrarenal

aneurysms," *Journal of vascular surgery*, vol. 68, no. 6, pp. 1706–1713, 2018.

[99] Rui Liao, Yunhao Tan, Hari Sundar, Marcus Pfister, and Ali Kamen, "An efficient graph-based deformable 2d/3d registration algorithm with applications for abdominal aortic aneurysm interventions," in *International Workshop on Medical Imaging and Virtual Reality*. Springer, 2010, pp. 561–570.

[100] Alexis Guyot, Andreas Varnavas, Tom Carrell, and Graeme Penney, "Non-rigid 2d-3d registration using anisotropic error ellipsoids to account for projection uncertainties during aortic surgery," in *International Conference on Medical Image Computing and Computer-Assisted Intervention*. Springer, 2013, pp. 179–186.

[101] Hossein Mohammadi, Simon Lessard, Eric Therasse, Rosaire Mongrain, and Gilles Soulez, "A numerical preoperative planning model to predict arterial deformations in endovascular aortic aneurysm repair," *Annals of biomedical engineering*, vol. 46, no. 12, pp. 2148–2161, 2018.

[102] Juliette Gindre, Aline Bel-Brunon, Adrien Kaladji, Aurélien Duménil, Michel Rochette, Antoine Lucas, Pascal Haigron, and Alain Combescure, "Finite element simulation of the insertion of guidewires during an evar procedure: example of a complex patient case, a first step toward patient-specific parameterized models," *International journal for numerical methods in biomedical engineering*, vol. 31, no. 7, pp. e02716, 2015.

[103] Atul Gupta, Subham Sett, Srinivasan Varahoor, and Ben Wolf, "Investigation of interaction between guidewire and native vessel using finite element analysis," in *Proceedings of the 2010 Simulia Customer Conference*, 2010.

[104] Ghizlane Mouktadiri and Benyebka Bou-Sa, "Aortic endovascular repair modeling using the finite element method," *Journal of biomedical science and engineering*, vol. 2013, 2013.

[105] David Roy, Gerhard A Holzapfel, Claude Kauffmann, and Gilles Soulez, "Finite element analysis of abdominal aortic aneurysms: geometrical and structural reconstruction with application of an anisotropic mate-

rial model," *The IMA Journal of Applied Mathematics*, vol. 79, no. 5, pp. 1011–1026, 2014.

[106] Adrien Kaladji, Aurélien Dumenil, Miguel Castro, Alain Cardon, Jean-Pierre Becquemin, Benyebka Bou-Saïd, Antoine Lucas, and Pascal Haigron, "Prediction of deformations during endovascular aortic aneurysm repair using finite element simulation," *Computerized medical imaging and graphics*, vol. 37, no. 2, pp. 142–149, 2013.

[107] Aurélien Duménil, Adrien Kaladji, Miguel Castro, Simon Esneault, Antoine Lucas, Michel Rochette, Cemil Göksu, and Pascal Haigron, "Finite-element-based matching of pre-and intraoperative data for image-guided endovascular aneurysm repair," *IEEE Transactions on Biomedical Engineering*, vol. 60, no. 5, pp. 1353–1362, 2012.

[108] Adrien Kaladji, Antoine Lucas, Alain Cardon, and Pascal Haigron, "Computer-aided surgery: concepts and applications in vascular surgery," *Perspectives in vascular surgery and endovascular therapy*, vol. 24, no. 1, pp. 23–27, 2012.

[109] Liang Liang, Minliang Liu, Caitlin Martin, John A Elefteriades, and Wei Sun, "A machine learning approach to investigate the relationship between shape features and numerically predicted risk of ascending aortic aneurysm," *Biomechanics and modeling in mechanobiology*, vol. 16, no. 5, pp. 1519–1533, 2017.

[110] Liang Liang, Minliang Liu, Caitlin Martin, and Wei Sun, "A deep learning approach to estimate stress distribution: a fast and accurate surrogate of finite-element analysis," *Journal of The Royal Society Interface*, vol. 15, no. 138, pp. 20170844, 2018.

[111] Liang Liang, Minliang Liu, Caitlin Martin, and Wei Sun, "A machine learning approach as a surrogate of finite element analysis–based inverse method to estimate the zero-pressure geometry of human thoracic aorta," *International journal for numerical methods in biomedical engineering*, vol. 34, no. 8, pp. e3103, 2018.

[112] Liang Liang, Wenbin Mao, and Wei Sun, "A feasibility study of deep learning for predicting hemodynamics of human thoracic aorta," *Journal of biomechanics*, vol. 99, pp. 109544, 2020.

[113] Song Wang, Brent Munsell, and Theodor Richardson, "Correspondence establishment in statistical shape modeling: Optimization and evaluation," in *Statistical Shape and Deformation Analysis*, pp. 67–87. Elsevier, 2017.

[114] Colin Goodall, "Procrustes methods in the statistical analysis of shape," *Journal of the Royal Statistical Society: Series B (Methodological)*, vol. 53, no. 2, pp. 285–321, 1991.

[115] Ferdinando Auricchio, Michele Conti, Matthieu De Beule, Gianluca De Santis, and Benedict Verhegghe, "Carotid artery stenting simulation: from patient-specific images to finite element analysis," *Medical engineering & physics*, vol. 33, no. 3, pp. 281–289, 2011.

[116] Geoffrey H White, Weiyun Yu, James May, Xavier Chaufour, and Michael S Stephen, "Endoleak as a complication of endoluminal grafting of abdominal aortic aneurysms: classification, incidence, diagnosis, and management," *Journal of Endovascular Therapy*, vol. 4, no. 2, pp. 152–168, 1997.

[117] Maria Antonietta Mazzei, Susanna Guerrini, Francesco Giuseppe Mazzei, Nevada Cioffi Squitieri, Dario Notaro, Gianmarco de Donato, Giuseppe Galzerano, Palmino Sacco, Francesco Setacci, Luca Volterrani, et al., "Follow-up of endovascular aortic aneurysm repair: Preliminary validation of digital tomosynthesis and contrast enhanced ultrasound in detection of medium-to long-term complications," *World journal of radiology*, vol. 8, no. 5, pp. 530, 2016.

[118] Johannes Boos, Olga R Brook, Jieming Fang, Nathaniel Temin, Alexander Brook, and Vasillios Raptopoulos, "What is the optimal abdominal aortic aneurysm sac measurement on ct images during follow-up after endovascular repair?," *Radiology*, vol. 285, no. 3, pp. 1032–1041, 2017.

[119] Frans L Moll, Janet T Powell, Gustav Fraedrich, Fabio Verzini, Stephan Haulon, Matthew Waltham, Joost A van Herwaarden, Peter JE Holt, Jasper W van Keulen, Barbara Rantner, et al., "Management of abdominal aortic aneurysms clinical practice guidelines of the european society for vascular surgery," *European journal of vascular and endovascular surgery*, vol. 41, pp. S1–S58, 2011.

[120] Boonprasit Kritpracha, Hugh G Beebe, and Anthony J Comerota, "Aortic diameter is an insensitive measurement of early aneurysm expansion after endografting," *Journal of Endovascular Therapy*, vol. 11, no. 2, pp. 184–190, 2004.

[121] Irene Bargellini, Roberto Cioni, Pasquale Petruzzi, Alessandro Pratali, Vinicio Napoli, Claudio Vignali, Mauro Ferrari, and Carlo Bartolozzi, "Endovascular repair of abdominal aortic aneurysms: analysis of aneurysm volumetric changes at mid-term follow-up," *Cardiovascular and interventional radiology*, vol. 28, no. 4, pp. 426–433, 2005.

[122] Jordan Knepper and Gilbert R Upchurch Jr, "A review of clinical trials and registries in descending thoracic aortic aneurysms," in *Seminars in vascular surgery*. Elsevier, 2010, vol. 23, pp. 170–175.

[123] Philipp Geisbüsch, Simone Hoffmann, Drosos Kotelis, Thomas Able, Alexander Hyhlik-Dürr, and Dittmar Böckler, "Reinterventions during midterm follow-up after endovascular treatment of thoracic aortic disease," *Journal of vascular surgery*, vol. 53, no. 6, pp. 1528–1533, 2011.

[124] Patricia Yau, Evan C Lipsitz, Patricia Friedmann, Jeffrey Indes, and Hasan Aldailami, "Aortic neck dilatation following thoracic endovascular aortic repair," *Annals of Vascular Surgery*, 2021.

[125] J Rueckel, P Reidler, N Fink, J Sperl, T Geyer, MP Fabritius, J Ricke, M Ingrisch, and BO Sabel, "Artificial intelligence assistance improves reporting efficiency of thoracic aortic aneurysm ct follow-up," *European Journal of Radiology*, vol. 134, pp. 109424, 2021.

[126] Viony M Belvroy, Hector WL De Beaufort, Joost A Van Herwaarden, Jean Bismuth, Frans L Moll, and Santi Trimarchi, "Tortuosity of the descending thoracic aorta: Normal values by age," *Plos one*, vol. 14, no. 4, pp. e0215549, 2019.

[127] A Ferrarini, A Finotello, G Salsano, F Auricchio, D Palombo, G Spinella, B Pane, and M Conti, "Impact of leg bending in the patient-specific computational fluid dynamics of popliteal stenting," *Acta Mechanica Sinica*, vol. 37, no. 2, pp. 279–291, 2021.